ROYAL SOCIETY OF CHEMISTRY

PAPER

Check for updates

Unveiling the cytotoxic and anti-proliferative potential of green-synthesized silver nanoparticles mediated by *Colletotrichum gloeosporioides*†

Priyamvada Gupta, [iD] ‡[a] Swati Singh, [iD] ‡[a] Nilesh Rai, [iD] [a] Ashish Verma, [iD] [a] Harshita Tiwari, [iD] [a] Swapnil C. Kamble, [iD] [b] Hemant Kumar Gautam [iD] [c] and Vibhav Gautam [iD] *[a]

Fungal endophytes are a putative source of bioactive metabolites that have found significant applications in nanomedicine due to their metabolic versatility. In the present study, an aqueous extract of the fungal endophyte, *Colletotrichum gloeosporioides* associated with a medicinal plant *Oroxylum indicum*, has been used for the fabrication of green silver nanoparticles (CgAgNPs) and further evaluated their cytotoxic and anti-proliferative activity. Bioanalytical techniques including UV-Vis spectral analysis revealed a sharp band at 435 nm and functional molecules from the aqueous extract involved in the synthesis of CgAgNPs were evidenced through FTIR. Further, the crystalline nature of CgAgNPs was determined through XRD analysis and microscopy techniques including AFM, TEM and FESEM demonstrated the spherical shape of CgAgNPs exhibiting a crystalline hexagonal lattice and the size was found to be in the range of 9–29 nm. The significant cytotoxic potential of CgAgNPs was observed against breast cancer cells, MDA-MB-231 and MCF-7 with IC_{50} values of 18.398 ± 0.376 and 38.587 ± 1.828 μg mL^{-1}, respectively. The biochemical study revealed that the treatment of MDA-MB-231 and MCF-7 cells with CgAgNPs reduces glucose uptake, suppresses cell proliferation, and enhances LDH release, indicating reduced cell viability and progression. Moreover, our research revealed differential expression of genes associated with apoptosis, cell cycle inhibition and metastasis suppression, evidencing anti-proliferative activity of CgAgNPs. The main objective of the present study is to harness anti-breast cancer activity of novel biogenic nanoparticles synthesized using the aqueous extract of *O. indicum* associated *C. gloeosporioides* and study the underlying mechanistic pathway exerted by these mycogenic nanoparticles.

[a]*Centre of Experimental Medicine and Surgery, Institute of Medical Sciences, Banaras Hindu University, Varanasi-221005, India. E-mail: vibhav.gautam4@bhu.ac.in; priyamvada.24@bhu.ac.in; swati.7672@bhu.ac.in; nilesh.rai17@bhu.ac.in; ashish.4@bhu.ac.in; harshitaruchi4218@gmail.com; Tel: +918860182113*

[b]*Department of Technology, Savitribai Phule Pune University, Ganeshkhind, Pune 411007, India. E-mail: sckamble@unipune.ac.in*

[c]*Department of Immunology and Infectious Disease Biology, CSIR-Institute of Genomics and Integrative Biology, Sukhdev Vihar, New Delhi 110025, India. E-mail: hemant@igib.res.in*

† Electronic supplementary information (ESI) available. Table S1. List of forward and reverse primers, and their sequences used in qRT-PCR analysis. Table S2. FTIR analysis of CgAgNPs. Fig. S1. Calibration curve of pyruvic acid for LDH assay. Fig. S2. FTIR spectrum of the aqueous extract of *C. gloeosporioides*. Fig. S3. Two dimensional (2D) AFM image showing the surface topography and dispersity of CgAgNPs. Fig. S4: Effect of CgAgNPs on viability of RAW 264.7 cells determined through MTT assay. The data is representative of three independent experiments. The statistical significance was determined through calculation of *p*-value where mean ± SEM of percentage cell viability of RAW 264.7 cells were compared using one-way ANOVA followed by Tukey. The statistical significance is represented as: ***$p \leq 0.001$; **$p \leq 0.002$; and *$p \leq 0.033$. See DOI: https://doi.org/10.1039/d3ra06145k

‡ Equal contribution.

1. Introduction

Over the past centuries, nanobiotechnology has remarkably served as a groundbreaking field in various sectors, including disease biology, engineering, chemical biology and more particularly, biomedicine.[1] Recently, nanomaterials-based theranostic approach which includes diagnosis and therapeutics, has surpassed the barriers faced in eradicating the cancerous cells.[2,3] These nanomaterials have inherent properties of microbicidal, anti-inflammatory, anticancer and antioxidant which have been extensively helpful in the manipulation of these nanoparticles in nanomedicine.[4] The screening of these nanomaterials in *in vitro* and *in vivo* biological systems have been achieved using different microscopy-based platforms and has greatly contributed in health and medicine.[5] The green-based synthesis of silver nanoparticles using microorganisms as biosynthetic machinery for the formulation of nanomaterials has gained enormous interest due to their eco-friendly, cost-effective and non-toxic nature and has also aided against various health ailments.[6] Fungal endophytes associated with

medicinal plants are prolific manufacturers of various bioactive compounds serving as antioxidant, antimicrobial, anti-diabetic, immunosuppressant and neuroprotective agents.[7–11] Moreover, these bioactive compounds derived from fungal endophytes also exhibit potential anticancer activities against several malignancies and thus lead to the discovery of many novel compounds.[12–15] The chemistry of these fungal endophyte derived compounds can be studied through several mass-spectrometry based methods coupled with bioinformatics tools so as to derive a descriptive account of their compositional structure and functional interpretation.[16,17] The pharmacologically important fungal compounds have also found their applications in nanotechnology and have been used for the development of nanodrugs against cancer.[18] The increased surface to volume percentage of silver suggests a better non-toxic, cost effective and eco-friendly approach for the fungal mediated formation of silver nanoparticles.[19] Thus, these fungi are considered as nano-factories for mycofabrication of nano-materials with controlled shape and size.[20,21] Plethora of evidences have suggested the potential role of myco-derived silver nanoparticles against inhibition of cancer proliferation, invasion and metastasis.[22–24]

Cancer, an unrestricted cell proliferation is considered as one of the leading and deadliest cause worldwide. Among all type of cancer, breast cancer is considered as the most common and second greatest cause of death after lung carcinoma. The most dangerous and aggressive type of cancer is triple negative breast cancer (TNBC) due to its poor prognosis, limited available treatments and metastatic property.[25] The tumor proliferation rate in most of the breast cancer type is directly proportional to the expression level of the estrogen receptor. Thus, MCF-7 cell which is non-invasive type of cancer cell contains functional epidermal growth factor (EGF) and estrogen receptors whereas, MDA-MB-231 cells are more aggressive hormone independent invasive type of TNBC.[26] According to the American Cancer Society, the breast cancer status reported globally among women has shown an estimate of 281 550 and 287 850 new cases of breast cancer in 2021 and 2022, respectively, showing an approximate 6300 rise and about 43 600 and 43 250 estimated deaths in 2021 and 2022, respectively that is predicted to happen in the United States.[27,28] The process of alterations in metabolism and bioenergetics of tumor cells called metabolic reprogramming is considered as one of the cancer hallmarks.[29] These prevalent changes in metabolism is essential for cellular growth and division of cancer cells which is required for malignant transformation, tumor invasion, unlimited proliferation, metastasis and enhanced survival capacity.[30] Previous literature showed that the depletion of glucose uptake by breast cancer cells have shown increased cytotoxicity therefore, significantly reduces proliferation rate in a dose dependent manner.[31] In a report, it has been demonstrated that glucose deprivation induces apoptosis in MCF-7/ADR breast cancer cells.[32] The activated status and enhanced expression profile of LDH in various cancers has contributed to explore diverse characteristic features of cancer malignancies. Abnormal upregulation of LDH leads to tumor progression through high lactate production, increased glycolysis, regulating ROS production and modulating various cancer associated proteins.[33] LDH is a cytosolic soluble enzyme that is released extracellularly upon impairment of cellular membrane. Therefore, its level in blood or serum could act as a signal of tissue damage.[34] Previous study has shown cytotoxic potential of AgNPs on human hepatoma cancer cells that significantly exhibited rise in LDH level.[35] Cell proliferation is a well distinct regulated process, critically essential in medical sector ranging from organogenesis in embryo to tissue repairment to carcinogenesis.[30] Recent reports have shown the anti-proliferative action of AgNPs on HeLa cells that exhibited maximum reduction of cell proliferation.[36] Deregulated cell proliferation and genomic alterations in malignant cells that abrogate normal signaling pathways governing cell cycle check-points, further facilitates the dysregulation of cell cycle.[37] Apoptosis, a major regulator of tumor progression is governed by oncogenes and tumor suppressor gene. Previous study revealed that biogenic AgNPs induces dysregulation in gene expression of pro-apoptotic and anti-apoptotic genes against HCT-116 colon cancer cells due to nuclear damage and disruption of the mitochondrial membrane.[38] Thus, the dysregulation in gene expression related to apoptosis could be considered as significant diagnostic markers in chemotherapy.[39] Many reports have demonstrated the role of fungal endophytes against breast cancer progression and thus have been emerged as an effective therapeutic approach over other treatment strategies.[40–42] Our previous findings showed ethyl acetate extract of fungal endophyte *C. gloeosporioides* isolated from *O. indicum* exhibits unique biochemical profile and potential cytotoxic activity.[43] Considering these findings, we have selected the fungal endophyte *C. gloeosporioides* for the synthesis of silver nanoparticles (CgAgNPs) and assessment of their cytotoxic and anti-proliferative properties against human breast cancer cells, MDA-MB-231 and MCF-7. Several bioanalytical methods such as UV-Vis, FTIR, XRD, AFM, TEM, FESEM and EDX have been used to characterize and validate the synthesis of CgAgNPs and results revealed their fcc lattice and size ranging between 9–29 nm. Further validation of *in vitro* cytotoxic and anti-proliferative potential of synthesized CgAgNPs was done using MTT assay followed by biochemical assays such as glucose estimation assay, cell proliferation assay and LDH assay. The expression level of several apoptosis-related genes revealed the molecular basis of anti-proliferative activity of CgAgNPs. The novel study shows first ever synthesis of silver nanoparticles mediated by *O. indicum* associated fungal endophyte *C. gloeosporioides* and assessment of the antiproliferative activity of green nanoparticles against breast cancer cells. The significant anti-breast cancer activity of CgAgNPs further urge to explore their anti-breast cancer mechanistic study through molecular elucidation so as to establish the novel CgAgNPs as a promising biotherapeutic agent.

2. Experimental procedure

2.1. Culturing and extraction of aqueous extract of *C. gloeosporioides*

The fungal strain, *C. gloeosporioides* was cultured in 100 mL of sterile PDB (Potato Dextrose Broth) media and fermentation was done at 26 ± 2 °C, for a week in an orbital shaker incubator

(100 rpm). The mycelial biomass was filtered using double layered cheesecloth and was rinsed in sterilized double distilled water (SDDW) to eliminate the traces of media content from the harvested mycelia. The collected fungal biomass (10 g) was added with 100 mL DDW for aqueous extraction and kept in an orbital shaker (100 rpm), at 28 ± 4 °C, for 24 hours. Finally, the aqueous filtrate, rich in fungal bioactive components was collected using Whatman No.1 filter paper and centrifuged to pellet down any suspended debris. The residual fungal mass was discarded and the supernatant was retained for AgNPs synthesis.

2.2. Mycosynthesis of AgNPs using fungal aqueous extract

For AgNPs synthesis, 1 mM silver nitrate ($AgNO_3$) was added to fungal aqueous extract and agitated on magnetic stirrer (350 rpm) in dark at 40 ± 4 °C for 24 hours. It was then centrifuged twice or thrice at 15 000 rpm for 15 minutes following washing with nuclease free water. The supernatant was discarded and the retained pellet containing the AgNPs was lyophilized and crushed to a fine powder. Subsequently, the powdered form of AgNPs was used for characterization and *in vitro* experiments.

2.3. Characterization of mycosynthesized silver nanoparticles (CgAgNPs)

The formation of AgNPs and their optical and morphological detection were investigated through characterization using different techniques including Ultraviolet-visible spectroscopy (UV-Vis), Fourier Transform Infrared Spectroscopy (FTIR), X-ray Diffraction (XRD), Atomic Force Microscopy (AFM), Transmission Electron Microscopy (TEM) and Field Emission Scanning Electron Microscopy (FESEM).

2.3.1. **Ultraviolet-visible spectroscopy (UV-Vis).** The analysis of the optical parameters of the biosynthesized AgNPs was monitored using Shimadzu Ultraviolet-Visible spectrophotometer (Kyoto, Japan) after visualizing the colour change. The as formed intense brown colour of the aqueous solution incubated with silver nitrate was then subjected to record the diffuse reflectance absorbance spectra at wavelength ranging from 200–700 nm at different time intervals.

2.3.2. **Fourier transform infrared spectroscopy (FTIR).** FTIR analysis was performed to study the surface chemistry of biogenic nanoparticles that gives an overview of functional biomolecules present in the fungal aqueous extract, involved in the synthesis of silver nanoparticles. The anchored functional bio constituents on the surface of the bioengineered nanoparticle were accountable for capping, stabilization as well as reduction of Ag^+ ions to AgNPs. The FTIR spectra of aqueous extract of *C. gloeosporioides* and biosynthesized AgNPs was scanned by the attenuated total reflectance (ATR) method at room temperature at wavelength ranging from 400–4000 per cm using an IR spectrophotometer (PerkinElmer). The obtained ATR-FT-IR spectra were compared with the findings of Coates study to validate the functional group of bioactive compound involved in the synthesis of CgAgNPs.[64]

2.3.3. **X-ray diffraction (XRD).** The crystallinity of the biosynthesized silver nanoparticles was investigated by Bruker model X-ray diffractometer (Advance Model-D8, Eco). The powdered form of bio-reduced AgNPs was coated on a sterilized glass silicon grid and the XRD measurements were carried out. Powder X-ray diffraction data were taken at 2θ scales in the range of 20°–80° operated at voltage 40 keV and current 20 mA. The Cu Kα act as source for X-ray radiation with λ value of 1.5418 Å. The obtained XRD data was analyzed using software Origin 2023. The determination of miller indices and the average particle size was calculated using X'pert High score plus software. The calculated miller indices were used to identify the Bragg's diffraction that helps in indexing XRD peaks. The AgNPs particle size was calculated by following Debye–Scherrer's equation.

$$D = \frac{K\lambda}{\beta \cos\theta}$$

where, D = crystallite domain size, K = Scherrer constant; θ = diffraction angle, β = peak width at half of its maximum height and λ = X-ray wavelength.

2.3.4. **Atomic force microscopy (AFM).** The detailed shape, size, morphology, agglomeration and surface coarseness of the biosynthesized AgNPs was revealed by AFM (NTEGRA Prima). It also delivers 3D image of the synthesized nanoparticle. The sample containing CgAgNPs was diluted in methanol, thereafter a drop of solution was placed onto the sterilized glass slide and kept for drying. AFM imaging was done at room temperature using phosphorus doped silicon cantilevers with frequency of 300 kHz and force constant 40 N m^{-1}. The presence of AgNPs was confirmed by the agglomeration of silver. The size of the particle was analyzed by Image J software whereas the surface topography (coarseness) of 2-D and 3-D images of formed nanoparticle was determined using Nova Px 3.2.5 software.

2.3.5. **Transmission Electron Microscopy (TEM).** The morphological characterization was done by Transmission Electron Microscopy (Tecnai G220 S-TWIN TEM) to get insight of the shape and size of the synthesized silver nanoparticles. The powdered CgAgNPs was dissolved in methanol followed by sonication. Thereafter, the sonicated suspension were put on the carbon grid functionalized with carbon and air dried in vacuum desiccators before analysis. Further, the images obtained were analyzed *via* Image J software to measure the diameter of the nanoparticles as well as to determine the particle size and distribution of polydisperse nanoparticles.

2.3.6. **Field emission scanning electron microscopy (FESEM).** FESEM analysis helps in identification of size, surface topography and 3-D image of the biosynthesized nanoparticles. The dried biosynthesized silver nanoparticle was coated over carbon tape and was analyzed at voltage 20 kV. The elemental composition and the surface topographical view of the biosynthesized nanoparticles at different magnification was evaluated through FESEM-EDX (Field Emission Scanning Electron Microscopy equipped with Energy-Dispersive X-ray) (Zeiss).

2.4. Maintenance of cell lines

The human breast cancer cells (MDA-MB-231 and MCF-7) and RAW 264.7 cells were cultured in Dulbecco's modified Eagle

medium (DMEM) supplemented with 10% heat inactivated fetal bovine serum (FBS), and 1% penicillin/streptomycin antibiotic solution and were maintained in a humidified 5% CO_2 incubator at 37 °C, until the cells get adhered and achieved 80–90% confluency.

2.4.1. Cell cytotoxicity assay. The cytotoxicity of the biosynthesized CgAgNPs against RAW 264.7 cells and breast cancer cells, MDA-MB-231 and MCF-7 was investigated through performing MTT assay.[44] The cultured cells were collected using trypsin–EDTA solution. Briefly, human breast cancer cells and RAW 264.7 cells were counted on Neubauer chamber and seeded at a density of 1×10^4 cells per well in a 96 well plate and incubated overnight in a humidified 5% CO_2 atmosphere at 37 °C until the cells get adhered. After incubation, cells were treated with varied concentration of CgAgNPs (5, 10, 25, 50, 100, and 200 μg mL^{-1}) and incubated overnight at 37 °C in 5% CO_2 incubator. Further, freshly prepared MTT solution (5 mg mL^{-1} dissolved in 1X PBS, pH 7.4) was added to the each well and incubated for 4 hours at 37 °C in 5% CO_2 incubator. The plate was centrifuged at 3000 rpm for 20 minutes. Finally, the resultant purple colored formazan crystals were dissolved in 100 μL of absolute dimethyl sulfoxide (DMSO) and absorbance was recorded at 570 nm using a microplate reader (ThermoFisher Scientific), and the data was analyzed statistically. The percent cell viability was calculated using the equation below:

$$\text{Cell viability}(\%) = \frac{\text{Absorbance (A570 nm) of treated sample}}{\text{Absorbance (A570 nm) of the control}} \times 100$$

2.5. Glucose estimation assay

The induction of growth inhibition and cytotoxicity in cancer cells is a well-known consequence of glucose deprivation. Considering the fact, we assessed the concentration of glucose in the culture media of MDA-MB-231 and MCF-7 cells treated with CgAgNPs (IC_{30}, IC_{50} and IC_{70} concentrations) using Glucose estimation kit (Beacon Diagnostics, India), as per manufacturer's protocol. The absorbance of control (non-treated) and CgAgNPs treated samples were measured against blank at 505 nm. The concentration of glucose was calculated and presented in mg dl^{-1} using the equation below and analyzed statistically:

$$\text{Concentration of glucose}(\text{mg dl}^{-1})$$
$$= \frac{\text{Absorbance of sample at 505 nm}}{\text{Absorbance of control at 505 nm}} \times 100$$

2.6. Cell proliferation assay

Cell proliferation assay helps in investigating the quantification of viable cells and proliferation rate using crystal violet.[45] In brief, the breast cancer cells, MDA-MB-231 and MCF-7 were treated with IC_{30}, IC_{50} and IC_{70} concentrations of CgAgNPs. After 24 hours of treatment, the media was discarded and the adhered cells were fixed with absolute ethanol for 10 minutes. Further, the fixed cells were stained with 0.05% crystal violet in 20% ethanol followed by 10 minutes of incubation. Further, the

cells were washed with distilled water followed by solubilization of formed crystals with methanol. The percent cell proliferation was then determined by taking absorbance at 595 nm using a microplate reader (ThermoFisher Scientific). The cell free medium was used as blank. The percent cell proliferation was calculated using the equation below:

$$\text{Cell proliferation }(\%) =$$
$$\frac{\text{Absorbance of sample at 595 nm}}{\text{Absorbance of control at 595 nm}} \times 100$$

2.7. Lactate dehydrogenase (LDH) assay

LDH assay is a calorimetric cytotoxicity assay that is used to quantify the intracellular LDH released from damaged plasma membrane into the extracellular culture medium. Briefly, breast cancer cells, MDA-MB-231 and MCF-7 were treated with IC_{30}, IC_{50} and IC_{70} concentrations of CgAgNPs. After 24 hours of treatment, the collected media was centrifuged at 3000 rpm for 3 minutes. The LDH rich supernatant was further used to estimate the LDH level using Lactate Dehydrogenase (LDH) activity assay kit (Elabscience), following the manufacturer's protocol. The absorbance of each sample was measured using microplate reader (ThermoFisher Scientific) at 450 nm. The LDH standard curve (Fig. S1†) was used to measure the level of LDH (U/L) and the obtained data was analysed statistically.

2.8. Evaluation of differential gene expression by real-time quantitative PCR (qRT-PCR)

The assessment of altered expression of apoptosis related genes in CgAgNPs treated breast cancer cells, MDA-MB-231 and MCF-7 was done using qRT-PCR analysis. The breast cancer cells, MDA-MB-231 and MCF-7 were treated with IC_{50} concentration of CgAgNPs. The treated cells were incubated overnight and maintained in a humidified 5% CO_2 atmosphere at 37 °C, followed by extraction of total RNA using TRIzol reagent. The extracted RNA was checked for its purity and concentration using Nanodrop (Thermo Scientific). The synthesis for cDNA was further done through reverse transcription of purified RNA following manufacturer's protocol provided in Thermo Scientific cDNA synthesis kit with some minor changes.[46] Moreover, following MIQE standard protocol,[47] qRT-PCR analysis was done with a PowerUp Thermo SYBR Green Master Mix and for the quantification, thermal cycles 5 real-time PCR system (Quant studio Thermo Fisher) was used. Different set of primers associated with apoptosis were used for screening the expression of genes (Table S1†). The mean C_T values were calculated for control and CgAgNPs treated samples and analysis was done by calculating $\Delta\Delta C_T$ value. Assessment of relative quantification of differentially expressed genes in terms of fold change was calculated by $2^{-\Delta\Delta CT}$ method.

2.9. Statistical analysis

All the experiments were performed in triplicate ($n = 3$). The data for MTT assay, glucose estimation, cell proliferation and LDH assay were expressed as mean ± SEM. The analysis of IC_{30},

IC_{50} and IC_{70} values for the MTT assay was done by using Graph Pad Prism 8.0.2 software. The one-way analysis of variance (one-way ANOVA) was used for the statistical analysis of all the data sets followed by Tukey's test (***$p \leq 0.001$; **$p \leq 0.002$; *$p \leq 0.033$). The data was expressed as mean ± SEM and respective values of all groups were compared. For qRT-PCR experiment, unpaired Student's t-test (*$p < 0.05$, **$p < 0.01$, ***$p < 0.001$) was used and mean ± SEM of all the groups were compared to determine the statistical significance using Graph Pad Prism 8.0.2 software.

3. Results and discussion

3.1. Bio-analytical techniques for the identification, characterization and evaluation of the synthesized nanoparticles

3.1.1. Confirmation of silver nanoparticle synthesis mediated by *C. gloeosporioides* (CgAgNPs) through visual inspection. The preliminary detection for the synthesis of silver nanoparticles was monitored through the colour change obtained after addition of $AgNO_3$ to the colourless fungal aqueous extract. Appearance of brown colour indicated the reduction of silver ions (Ag^+) into AgNPs (Ag^0), and thus formation of silver nanoparticles (Fig. 1A). The interesting bright colours of metal nanoparticles are due to the localized surface plasmon resonance (SPR). The surface plasmon resonance arise due to the movement of free electrons in metallic nanoparticles through conduction and valence band.[48] The characteristic dark reddish-brown colour in aqueous solution of AgNPs are related to the phenomenon of SPR[49] and that shows characteristic absorbance ranging from 400 nm to 450 nm.[48] With the increase in time duration, the colour got intensified and that marks the reduction of silver ions. Fungal endophytes are enormous producers of bioactive compounds owing to which they mediate the bioreduction of silver. The crude extract of fungal endophyte *C. gloeosporioides* as well as the derived purified compound have been reported in previous studies to possess interesting biological activities in terms of antioxidant and anticancer.[43,50,51] The aforesaid fungal endophyte has been extensively studied and have been validated for the presence of active components that could play a key role in silver nanoparticle synthesis. The enzymatic synthesis of silver nanoparticles has provided a range of nanoparticles with different chemical compositions, sizes and surface topology. In one of the previous reports, structurally and chemically different nanoparticles have been synthesized using phytochelatin and α-NADPH-dependent nitrate reductase purified from *F. oxysporum*.[52] Another report also demonstrated bioreduction of silver ions mediated by *F. oxysporum*.[53] The biosynthesis of silver nanoparticles using extract of *Fusarium acuminatum* Ell. and Ev (USM-3793) showed broad distribution of silver nanoparticles.[54] Stable silver nanoparticles produced from *Aspergillus flavus* with no aggregation, attributed to the bioactive compounds derived from the fungal endophyte which binds to the surface and act as stabilizing material.[55]

3.1.2. UV-Vis spectroscopy revealed optical parameters of CgAgNPs. The initial monitoring of the mycofabricated CgAgNPs was further confirmed by recording absorbance of the formed brown colour solution using UV-Vis spectrophotometer. The UV-Vis absorbance spectrum of the bioreduced Ag ions at different time intervals (2, 6, 12 and 24 hours) were recorded at wavelength ranging from 200–700 nm. This led to the initial characterization of synthesized CgAgNPs. The absorbance spectrum revealed a gradual rise of the peak with increase in incubation time that depicts the formation of silver nanoparticles at a wavelength range of 400–450 nm due to enhanced oscillations of electronic charges on nanoparticle surface known as Surface Plasmon Resonance (SPR) (Fig. 1B). The active phytoconstituents rich biomolecules present in the aqueous extract of mycelial biomass results in the conversion of silver ion (Ag^+) to silver metal (Ag^0) thus leading to the formation of AgNPs. UV-Vis spectrophotometer analysis has displayed a characteristic peak with λ_{max} at 435 nm due to localized surface plasmon resonance (LSPR) stimulation of the formed nanoparticle. The broad SPR band revealed the polydisperse nature of synthesized CgAgNPs. The excitation of free electrons present on metal surface leads to characteristic absorption spectra in the ultraviolet visible region. The induction of plasmon resonance arises when light photons of a particular frequency led to collective electronic oscillation in the conduction band region on the surface of nanoparticle.[56] The excitation of light quanta and peak formation shows significant effect on particle size of the mycosynthesized nanoparticle. The macroscopic change in colour during reduction process also impact the formation of different sizes of synthesized nanoparticle.[57] The NADH dependent nitrate reductase enzyme results in coating and stabilizing the formed nanoparticle.[58] The increase in incubation time corresponds to change in intensity of brown colour as well as increase in absorbance. Previous studies revealed the synthesis of *Colletotrichum* sp. ALF2-6 mediated AgNPs and was validated by using UV visible spectral analysis with peak ranges between 300 nm to 600 nm and λ_{max} at 425 nm.[59] The UV spectra analysis of the biosynthesized silver nanoparticle by entomogenous fungus, *Beauveria bassiana* has marked the electronic induction of plasmon resonance band at wavelength 430 ± 1.5 nm.[60]

3.1.3. FTIR revealed functional groups of fungal biomolecules mediating CgAgNPs synthesis. FTIR analysis demonstrated the existence of possible myco-associated phytochemicals involved in the biogenic synthesis of CgAgNPs and the spectra has been represented in Fig. 1C. The biomolecules present in aqueous extract of fungal filtrate were confirmed by FTIR. The evidence from the previous reports suggest that the associated bioactive compounds such as derivative of carboxylic acid and amino group present in protein molecules help in capping, stabilization and bio-reduction of synthesized nanoparticles.[61] The spectrum of aqueous extract of fungal endophyte before AgNPs formation (Fig. S2†) reveals characteristic strong absorption bands at 3306.95 cm^{-1}, 1635.44 cm^{-1}, 415.09 cm^{-1}, 435 cm^{-1} and 451.66 cm^{-1}. The significant band broadening at 3306.95 cm^{-1} is due to O–H (hydroxy) stretching whereas the bands at 1635.44 cm^{-1} corresponds to vibrational bending of primary amine. The absorption bands corresponding to the hydroxyl and amide groups of the fungal aqueous extract, shifted to lower wavenumber values from
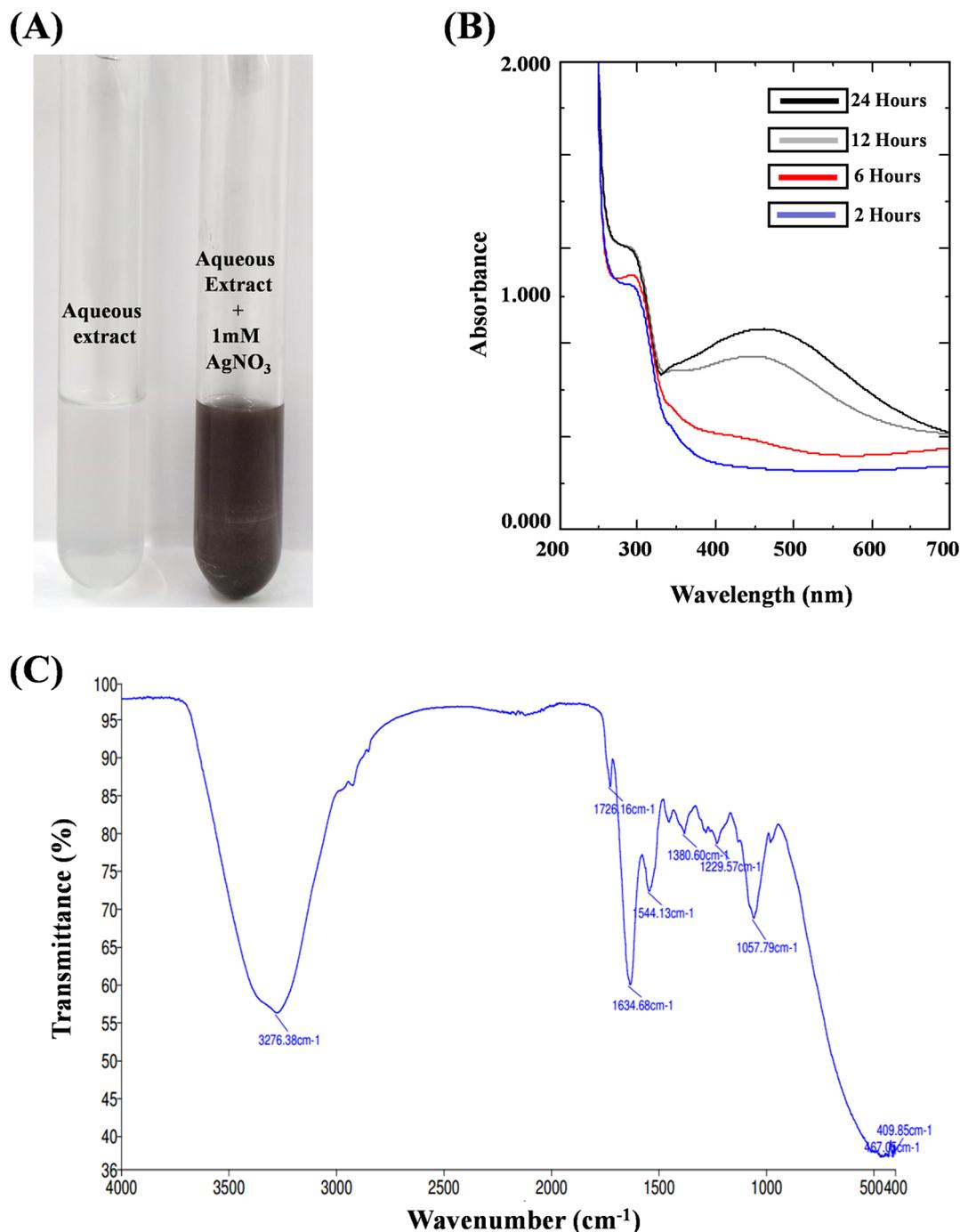
Fig. 1 Characterization of synthesized silver nanoparticles through recording optical spectra and FTIR spectroscopic measurements. (A) The bioreduction of silver ions was observed through change in the colour of aqueous extract from pale yellow to brown colour after addition of 1 mM silver nitrate (B) Absorption measurements using UV-Vis Spectrophotometer exhibited characteristic absorption maxima between 400–450 nm (C) FTIR spectrum of mycogenic silver nanoparticles revealed footprints of functional groups involved in the synthesis of silver nanoparticles.

3306.95 cm^{-1} to 3276.38 cm^{-1} and from 1635.44 cm^{-1} to 1634.68 cm^{-1} due to the association with silver nitrate (AgNO$_3$) solution. The gradual change in peak intensity is due to the reduction process that leads to the formation of AgNPs. Additionally, for CgAgNPs, bands were observed at 1726.16 cm^{-1} that corresponds to aldehydic functional group associated with C–H

stretching. The evidence from previous literature has shown the strong association ability of hydroxyl as well as carbonyl group with the formed nanoparticle acting as a capping and stabilizing agent.[62,63] The peaks observed at 1544.13 cm^{-1} and 1380.60 cm^{-1} are assigned to aliphatic or aromatic nitro compounds due to NO$_2$ stretch and C–H bending of methyl as

a functional group, respectively. The peaks at 1229.57 cm^{-1}, 1057.79 cm^{-1} and 467.05 cm^{-1} are assigned to vibrational P–O–C stretching due to presence of aromatic phosphate group, C–O vibrational stretching of alkyl substituted ether and S–S vibrational bending of aryl disulphides, respectively.[64] The list of bands observed for FTIR analysis of CgAgNPs has been represented in Table S2.† Consequently, the present data reveals that fungal associated proteins quickly wrap around AgNPs through protein's free hydroxyl, carboxyl and free amino groups that further contributes in stability of the formed nanoparticle. From previous reports, it has been evidenced that the FTIR spectra of *Penicillium* sp. mediated synthesized nanoparticle shows eight peaks that correlates to the existence of protein molecules as stabilizing and reducing agent due to planar amide I and amide II and binding vibrations of N–H, C–H and C–N stretching.[65] In another study, it has been reported that the FTIR analysis of the mycomediated fungal enzymatic filtrate contains cysteine residues, free amino and carboxyl groups that shows binding interaction with the formed nanoparticle thus validating the existence of protein as a stabilizing agent.[66]

3.1.4. XRD revealed crystalline nature and size of CgAgNPs. X-ray diffraction was done to estimate the crystallite nature, size as well as purity of the formed CgAgNPs. XRD graph was plotted against the peak intensity of the X-ray and the Bragg's reflection planes of 2θ values exhibiting 9 different peaks at 2θ value that corresponds to the orientation of silver. The average crystallite size was determined by Scherrer's equation. As crystallite domain size is inversely proportional to the width of the peak thus with smaller sizes, slight broadening in peak can be observed. Therefore, the characterization of the nanoparticles significantly effects the size dependent broadening of the XRD peak. XRD analysis shows the crystalline nature of CgAgNPs and average size has been estimated to be 10 nm. X-ray diffractogram is depicted in Fig. 2A which reveals the crystallinity and formation of the biosynthesized silver nanoparticles. The diffraction peak indexing to the 110 – plane show more intensity than other planes. The prominent peak at lattice planes (110) demonstrated the efficient synthesis of nanoparticles CgAgNPs. The XRD analysis depicts several diffraction patterns of the indices which corresponds to the Bragg reflection at 2θ, that is, 110 (32.426), 110 (33.545), 111 (36.834), 200 (46.397), 210 (48.073), 211 (52.95), 211 (55.39), 211 (6.617) and 310 (72.271). The crystallographic orientation of the nanoparticle can be estimated by *hkl* (Miller indices) values. The reflection planes value shows characteristic resemblance with the face centered cubic (fcc) after JCPDS (file no.-89-3722) analysis. According to the previous report, *Aspergillus sydowii* mediated AgNPs synthesis exhibited crystalline nature with average particle size of 12 ± 2 nm.[67] The XRD analysis of mycosynthesized nanoparticle by fungus *Penicillium verrucosum* further confirmed the crystalline nature of nanoparticles and the observed diffraction peak are in correspondence with Bragg reflections.[68]

3.1.5. AFM revealed 3-D surface roughness and topology of CgAgNPs. AFM analysis was done to study the size, agglomeration, shape, topology and surface coarseness of the biogenically synthesized silver nanoparticles. The characterization of the nanoparticle's bimodal distribution was reported by AFM.

The 2-D (Fig. S3†) and 3-D (Fig. 2B) images have revealed the well-dispersed slightly aggregated and homogenously shaped silver nanoparticles. The AFM analysis showed spherical shape of the synthesized nanoparticle. The Image J software was used to determine the average particle size and was reported to be 15 nm. The interpretation of several topographical features was further analyzed by measuring root mean square roughness (R_q) and average roughness (R_a) that determines the amplitude profile of the formed nanoparticles. The R_q and R_a value of spherically shaped CgAgNPs was found to be 20.206 nm and 14.302 nm, respectively. In addition to R_q and R_a, the shape parameters such as skewness (Rsk) and kurtosis (Rku) determine the asymmetrical height distribution and surface roughness of the CgAgNPs was found to be 1.615 and 5.97, respectively. A previous report of the AFM analysis has shown small size of the biogenic silver nanoparticles in the range of 36–46.5 nm, with an average particle size of 46.5 nm.[69] The fabrication of silver nanoparticles from fungal endophyte *Raphanus sativus* revealed round shaped particle of mean size between 4–30 nm.[70]

3.1.6. TEM revealed geometric shape and size of CgAgNPs. The morphological characterization of shape and size of mycofabricated CgAgNPs were elucidated through TEM. The micrograph has shown polydisperse nature of biosynthesized nanoparticles with relatively spherical shape and least aggregation at scale of 50 nm (Fig. 2C). The analysis of TEM histogram of the synthesized CgAgNPs by Image J software revealed polydisperse nature with size ranging from 9–29 nm showing average particle size of 17 nm (Fig. 2D). The homogeneity of the nanoparticles was due to the polyphenols released from the aqueous extract of *C. gloeosporioides* that act as capping and reducing agent (which reduces silver ions to silver metal). In one of the report, TEM analysis has shown the polydisperse and spherical nature of the silver nanoparticle synthesized from *Aspergillus terreus* with size ranging from 1–20 nm with an average particle size of 4.3 nm.[71] Our findings corroborate with a previous study, showing the spherical shape of the nanoparticle synthesized using *F. acuminatum* exhibited a size distribution ranging from 5–40 nm, with an average size of 13 nm.[54]

3.1.7. FESEM revealed surface topology and elemental composition of CgAgNPs. The chemical composition, shape and morphology of the mycomediated synthesized CgAgNPs was examined using FESEM. The images recorded at scale of 200 nm and magnification of 100.00 KX has revealed topographical view showing more or less spherical shaped nanoparticles that are clustered together bearing rough surface (Fig. 2E). EDX spectroscopic analysis revealed sharp and strongest absorption peak for silver (Ag) at 3 keV that verifies its presence as the mycosynthesized silver nano-crystallites exhibiting characteristic plasmon resonance while the weaker signal for carbon and oxygen were also observed. In one of the report, the characteristic peak of AgNPs synthesized by *P. oxalicum* was at 3 keV showing compatibility with the present work.[72] The chemical characterization of the element was performed by energy disperse X-ray based on sample interaction with the excitation of X-ray that reveals certain peaks corresponding to different energy levels. Each peak corresponds to specific
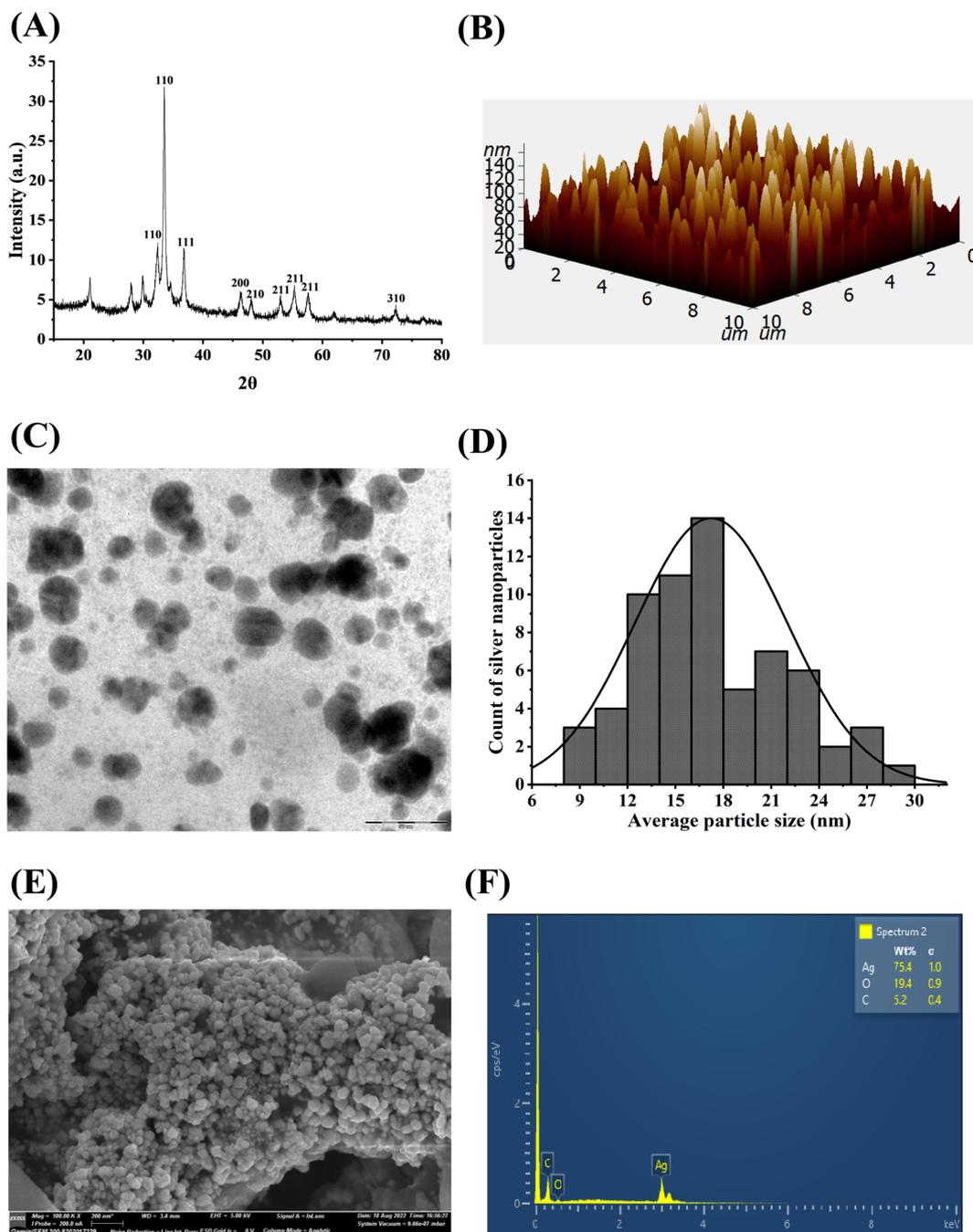
Fig. 2 Bio-analytical techniques for the characterization of nano-silver particles (CgAgNPs). (A) XRD spectrum showing crystalline nature of CgAgNPs. (B) 3-D AFM image of CgAgNPs showing well-dispersed homogeneously shaped nanoparticles. (C) TEM images of biosynthesized silver nanoparticles showing uniformity in shape and dispersion. (D) Particle size distribution pattern of synthesized green nanoparticles. (E) FESEM micrographs detailing shape, size and distribution of mycosynthesized CgAgNPs. (F) EDX profile showing characteristic signal indicating corresponding biosynthesized silver nanoparticles.

element present in fungal aqueous filtrate. The spectrum is plotted against cps eV^{-1} (count per second per electron Volt) *vs.* keV (kinetic energy of electrons in beam). The EDX chart analysis of the nature and chemical composition of CgAgNPs has shown silver (Ag) as the core element having percentage as 75.4% which confirmed the reduction of silver ions. The FESEM-EDX profile of mycofabricated AgNPs is shown in Fig. 2F. Some other elements such as C and O atom has also been captured showing weaker signals with 5.2% and 19.4%, respectively. Further, FESEM micrograph confirms that the released phytochemicals from the fungus *C. gloeosporioides* act as potent stabilizer and reducing agent with least cluster of the formed nanoparticle.[73] SEM analysis through past researches has revealed uniformly-distributed, spherical, monodispersed and least agglomerated nanoparticles synthesized by *Cladosporium cladosporioides*.[74] The microstructural and

morphological analysis through SEM and EDX profiling has shown spherical and agglomerated nature of the biogenically formed silver nanoparticle by *Alternaria alternata* as well as showed characteristic silver peak at 3 keV that indicates silver nanoparticle absorption due to plasmon resonance effect.[75]

3.2. CgAgNPs exhibited potential *in vitro* cytotoxicity against breast cancer cells

The cytotoxicity of biosynthesized silver nanoparticles was evaluated against RAW 264.7 cells and two breast cancer cells, MDA-MB-231 and MCF-7 and the inhibitory concentration at half maximal (IC_{50}) that is required to inhibit the cancer cells proliferation by 50% as compared to the control was calculated. The anti-proliferative activity of CgAgNPs was tested at different concentrations (5, 10, 25, 50, 100 and 200 μg mL^{-1}) using MTT assay and percentage cell viability was calculated and represented in form of histogram for RAW 264.7 cells (Fig. S4†) and breast cancer cells (Fig. 3). The result analysis clearly indicates the significant cytotoxic action of CgAgNPs against breast cancer cells, MDA-MB-231 and MCF-7 while, toxicity against RAW 264.7 cells was observed at very higher dose. The spectrophotometric analysis indicates the decrease in percent cell viability with increase in CgAgNPs concentration. For MDA-MB-231 and MCF-7 cells, the calculated IC_{50} value, where cell viability was reduced to 50% after CgAgNPs treatment, was found to be 18.398 ± 0.376 and 38.587 ± 1.828 μg mL^{-1}, respectively, however, for RAW 264.7 cells it was found to be 195.221 ± 2.394 μg mL^{-1}. The synthesized CgAgNPs showed high cytotoxicity to MDA-MB-231 and MCF-7 cells at low dose while represent biosafety towards healthy cells. Moreover, IC_{30} and IC_{70} values of CgAgNPs were also calculated as 8.487 ± 0.065 and 65.678 ± 2.571 μg mL^{-1}, respectively for MDA-MB-231 cells and for MCF-7 it was reported as 8.839 ± 0.398 (IC_{30}) and 180.61 ± 4.551 μg mL^{-1} (IC_{70}). Various mechanisms contribute to the cytotoxic activity of the synthesized CgAgNPs, including cellular disintegration, buildup of free radicals (ROS & RNS), damage to nucleic acid and degradation of surface protein. As the wrapped silver particle (Ag) get released from the bounded fungal filtrate moiety, they start piling up on the targeted sites that obstructs in electron transport system ultimately causing efflux of intracellular ion and damage to cell.[76] A previous study has reported in accordance with the present data that depicts the potential cytotoxic action at IC_{50} value (8.7 μg mL^{-1}) against MDA MB-231 cells treated with biosynthesized AgNPs from *B. funiculus*.[77] The synthesis of AgNPs from leaf extract of *C. edulis* exhibited concentration dependent cytotoxicity on mammalian cells (L929).[78] Considering the cytotoxic potential of CgAgNPs against breast cancer cells, subsequent experiments have been performed to study the anti-proliferative potential of CgAgNPs.

3.3. CgAgNPs inhibited glucose uptake in breast cancer cells

The quantification of glucose content in culture media of CgAgNPs treated breast cancer cells was done to evaluate the metabolic alteration induced by CgAgNPs. After treatment with the respective concentration of CgAgNPs (IC_{30}, IC_{50}, and IC_{70}) compared with respect to control, the glucose content was significantly increased in a dose dependent manner (Fig. 4A and B). As glucose deprivation adversely inhibits the cell growth, therefore, the amount of glucose present in culture media of CgAgNPs treated breast cancer cells was analyzed that helps in the quantification of the glucose consumption. The culture media of control groups for both the cells, MDA-MB-231 and MCF-7 exhibited very low glucose content, measuring 22.309 ± 0.238 and 27.117 ± 0.235 mg dl^{-1}, respectively as compared to treated group. The glucose content in culture media of MDA-MB-231, administered with different doses of CgAgNPs (IC_{30}, IC_{50} and IC_{70}) were found to be 30.096 ± 0.063, 36.539 ± 0.146 and 42.021 ± 0.296 mg dl^{-1}, respectively, whereas in culture media of MCF-7 cells was found to be 30.384 ± 0.122, 32.789 ± 0.409 and 38.846 ± 0.409 mg dl^{-1}, respectively. The result analysis revealed that in culture media of breast cancer cells treated with CgAgNPs at higher dose of IC_{70} exhibits high glucose content, indicating reduced cell viability, proliferation and altered metabolic activity. Previous findings have reported that AgNPs substantially altered the glucose metabolism in hepatoma cells (HepG2) by reducing the glucose consumption cancer cells.[79] The glucose availability in AgNPs treated HepG2 cells has shown that low level of glucose supply induces ROS generation in cancer cells.[80] Hence, the finding suggest that reduced glucose uptake may act as regulatory point to precisely target tumor cells while reducing adverse effects on healthy cells.

3.4. CgAgNPs significantly inhibited cell proliferation in breast cancer cells

The cell proliferation assay by crystal violet dye that generally stains adherent cells helps in the determination of proliferation and viability of the cultured cells. Upon treatment with the different concentration of CgAgNPs, the adhered cells undergo cell death and lose adherence. The concentration-dependent cell abundance was determined by crystal violet dye that generally binds to nucleic acid and proteins of adhered cultured cells. This leads to indirect quantification of non-viable cells and helps in determination of cell proliferation rate. Cells that have undergone cell death, lose adherence property and therefore significantly colour intensity of crystal violet dye is reduced.[81] According to the fact, after treatment of MDA-MB-231 and MCF-7 cells with respective IC_{30}, IC_{50}, and IC_{70} concentration of CgAgNPs, we further sighted to determine the percent cell proliferation of the adhered cells. The CgAgNPs at different inhibitory concentration of IC_{30}, IC_{50} and IC_{70} showed dose-dependent decrease in cell proliferation rate in breast cancer cells (Fig. 4C and D) which was in accordance with the result of MTT assay. For MDA-MB-231 cells, the percent cell proliferation treated with IC_{30}, IC_{50} and IC_{70} concentrations of CgAgNPs was found to be 94.878 ± 0.459, 63.63 ± 0.230 and $13.98 \pm 0.483\%$, respectively as compared to control. Whereas, for MCF-7 cells, the percent cell proliferation was found to be 93.183 ± 0.426, 24.708 ± 0.661 and $17.463 \pm 0.571\%$, respectively. Cell proliferation is a highly regulated process of normal cells. Lack of contact inhibition, alters protein expression related to cell cycle as well as morphological transitions of epithelial cells contribute to uncontrolled proliferation of cancer cells.[82]
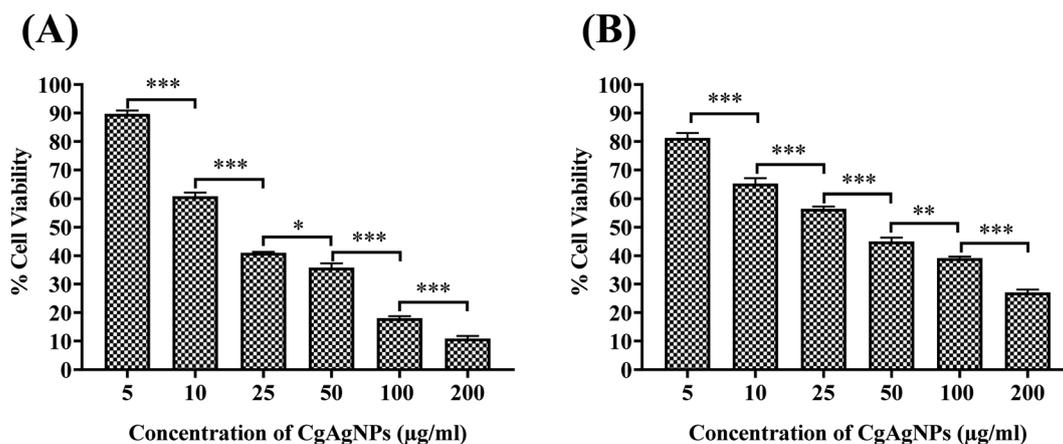
MDA-MB-231

MCF-7

Fig. 3 Cytotoxic effects of CgAgNPs against (A) MDA-MB-231 (B) MCF-7 human breast cancer cells. The data is representative of three independent experiments. The statistical significance was determined through calculation of p-value where mean $\pm$ SEM of percentage cell viability of the human breast cancer cells were compared using one-way ANOVA followed by Tukey. The statistical significance is represented as: ***$p \leq 0.001$; **$p \leq 0.002$; and *$p \leq 0.033$.

Similarly, previous researches has shown HCT116 cells treated with AgNPs exhibited significant anti-proliferative action.[83] The AgNPs synthesized from *Abutilon indicum* exhibited remarkable anti-proliferative action against colon cancer cells (COLO 205).[84] Collectively, the findings revealed that CgAgNPs induces significant decrease in cell proliferation in a concentration dependent manner.

3.5. CgAgNPs enhanced LDH release in breast cancer cells

LDH assay determines the cytotoxic effect against the breast cancer cells and degradation of cellular integrity after treatment with CgAgNPs. The effect of CgAgNPs treatment on LDH activity in culture media of breast cancer cells was monitored by changes in absorbance at 450 nm during NAD^+ reduction. Compared to control, the treated groups showed more toxicity as validated by high LDH activity in culture media (Fig. 4E and F). CgAgNPs treated breast cancer cells (MDA-MB-231 and MCF-7) causes decreased cytosolic LDH level which shows decrease in proliferation rate in a dose dependent manner. CgAgNPs induces damage to the membrane of cancer cell that leads to the release of cytosolic LDH to the supernatant. The treated cells displayed high level of released LDH as compared to the untreated cells. CgAgNPs at different concentration of IC_{30}, IC_{50} and IC_{70} showed dose-dependent rise of LDH activity in culture media of breast cancer cells, MDA-MB-231 and MCF-7. In the culture media of MDA-MB-231 cells, the LDH activity at different concentrations of CgAgNPs that is IC_{30}, IC_{50} and IC_{70} was found to be 186.731 ± 1.411, 286.084 ± 2.334 and 339.806 ± 1.483 U L^{-1}, respectively as compared to control (177.67 ± 1.682 U L^{-1}). Whereas, for culture media of CgAgNPs treated MCF-7 cells, the LDH activity at different concentrations of IC_{30}, IC_{50} and IC_{70} was found to be 237.864 ± 1.682, 353.074 ± 1.802 and 393.204 ± 2.201 U L^{-1}, respectively as compared to control (184.79 ± 0.856 U L^{-1}). During cellular damage, LDH being

a soluble cytosolic enzyme gets released into the media and that is indicative of increased cytotoxicity. LDH promotes the conversion of lactate into pyruvate *via* reduction of NAD^+ into NADH which further reacts with chromogenic substrate that show colour change. The histogram obtained for LDH activity and MTT assay reveals inverse relationship that validates the cytotoxicity of bio-fabricated CgAgNPs. In both MTT and LDH assay, with rise in CgAgNPs concentration we found substantial rise in cytotoxic level which was confirmed by measuring percent cell viability and LDH level, respectively. Previous studies has revealed the potential cytotoxic action of AgNPs on lung cancer cells (A549) that caused damage to cell membrane with LDH release in a dose dependent manner.[85] The biogenically synthesized AgNPs from *L. boronitolerans* has shown significant cytotoxic action against C2C12 muscle cell line that leads to distortion of cellular membrane in a concentration dependent manner.[86] Therefore, the result validates that green synthesized nanoparticles CgAgNPs can serve as a potential cytotoxic as well as anti-proliferative agent against the breast cancer cells.

3.6. CgAgNPs treated breast cancer cells exhibited altered gene expression

Apoptosis is a key regulator of tissue homeostasis as well as highly regulates the process of tumorigenesis by causing cell death.[87] The breast cancer cells (MDA-MB-231 and MCF-7) treated with CgAgNPs were investigated for the differentially expressed genes in control and treated groups. The molecular approach guiding CgAgNPs induced apoptosis in MDA-MB-231 and MCF-7 cells were determined by examining the fold change expression levels of apoptosis related genes (*BAX*, *BCL-2*, *P21*, *P53* and *FADD*) as shown in Fig. 5A and B. The qRT-PCR data analysis has revealed upregulation of pro-apoptotic gene, *BAX* in MDA-MB-231 and MCF-7 cells with fold increase of 1.242 ± 0.117 (p-value 0.175)
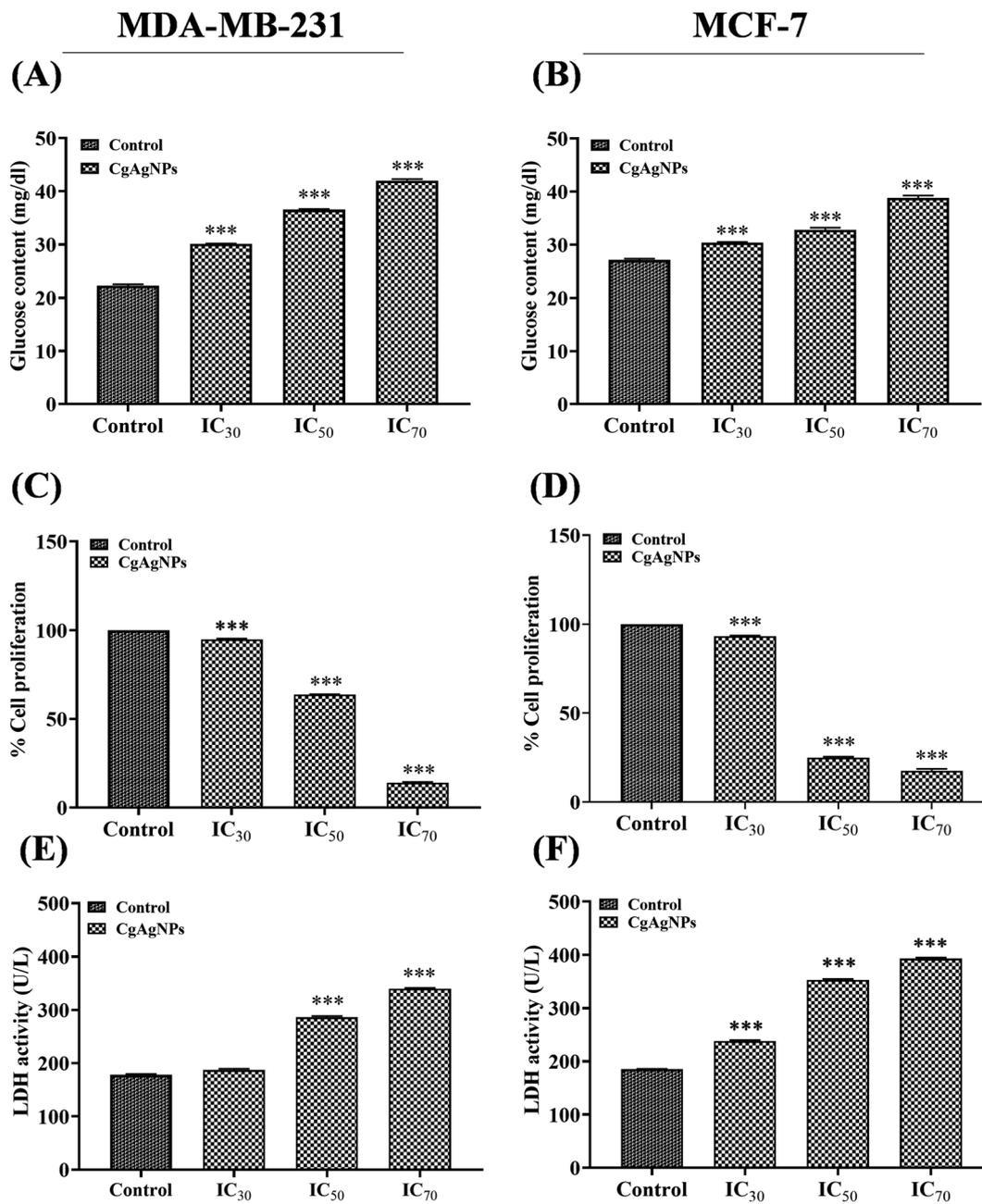
MDA-MB-231   **MCF-7**

Fig. 4 Anti-proliferative and cytotoxic study using different biochemical parameters responsible for mediating cell proliferation, metastasis and invasion in human breast cancer cells, MDA-MB-231 and MCF-7. (A) and (B) Glucose content increased in a dose-dependent manner as a resultant of reduced glucose metabolism and cell death. (C) and (D) The % cell proliferation was attenuated under the effect of CgAgNPs and, (E) and (F) LDH release was induced in a concentration-dependent manner. The data is representative of three independent experiments. The statistical significance was determined through calculation of p-value where mean ± SEM of glucose content, cell proliferation and LDH level in control was compared with CgAgNPs treated human breast cancer cells using one-way ANOVA followed by Tukey. The statistical significance is represented as: ***$p \leq 0.001$; **$p \leq 0.002$; and *$p \leq 0.033$.

and 3.315 ± 0.093 (p-value 0.002), respectively with respect to control. In MCF-7 cells, the *BAX* gene expression shows statistically significant difference between control group and treated group. The cell cycle growth regulator, *P21* was found to be upregulated with fold increase of 1.223 ± 0.065 (p-value 0.075) and 3.714 ± 0.112 (p-value 0.002) in MDA-MB-231 and MCF-7 cells, respectively with respect to control, showing statistically significant difference in MCF-7 cells only. The tumor suppressor gene, *P53* showed upregulation with fold increase of 1.299 ± 0.065 (p-value 0.044) and 2.994 ± 0.363 (p-value 0.032) in MDA-MB-231 and MCF-7 cells, respectively showing statistical difference in both the treated cells with respect to control. In MDA-MB-231 and MCF-7 cells, the *FADD* gene also gets upregulated with respect to control and having fold increase of 1.202 ± 0.049 (p-value 0.054) and 2.899 ± 0.149 (p-value 0.006), respectively showing statistically significant difference in MCF-7 cells only.
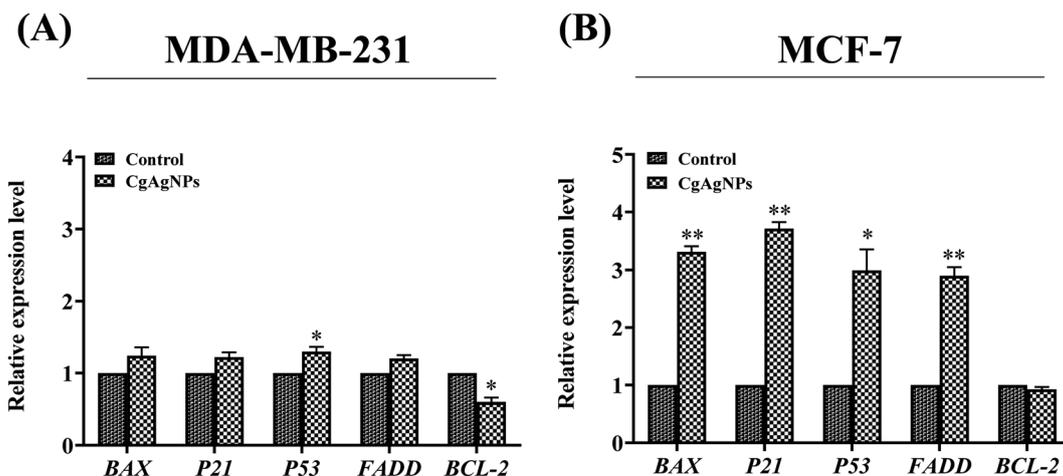
Fig. 5 Graphical representation of CgAgNPs induced differential gene expression in human breast cancer cells. The human breast cancer cells, (A) MDA-MB-231 and (B) MCF-7 treated with IC_{50} concentration of CgAgNPs induced upregulation of proapoptotic gene *BAX* and *FADD*, cell-cycle arrest gene *P21*, tumor suppressor gene *P53* and, downregulation of anti-apoptotic gene *BCL-2*. The data is representative of three independent experiments. The statistical significance was determined through calculation of *p*-value where mean $\pm$ SEM of relative mRNA expression were compared using the unpaired Student's *t*-test. The statistical significance is represented as: ***$p \leq 0.001$; **$p \leq 0.002$; and *$p \leq 0.033$.

CgAgNPs treated cells showed enhanced expression of *P53* that possibly indicates activation of apoptosis signaling pathway through conformational changes in amino terminal of mitochondrial membrane that triggers release of cytochrome c.[88] The anti-apoptotic gene, *BCL-2* shows downregulation by 0.599 ± 0.061 (*p*-value 0.022) and 0.924 ± 0.041 (*p*-value 0.205) fold in MDA-MB-231 and MCF-7 cells, respectively showing statistically significant difference in MDA-MB-231 cells only with respect to control. The tumor suppressor gene, *P53* modulate the process of apoptosis by its activation through regulation of Bcl-2 family members. These protein family comprises both pro-apoptotic gene, *BAX* as well as anti-apoptotic gene *BCL-2*.[89] The heterodimerization of Bax (Bcl-2 associated *X*) protein and Bcl-2 shows structural sequence homology that triggers apoptosis by causing membrane permeabilization in mitochondria causing release of cytochrome c into the cytosol that further stimulate caspases and p53 to induce apoptosis.[90] The downregulation of *BCL-2* by CgAgNPs suggests cell death by directly binding and suppressing pro-apoptotic Bcl-2 family proteins through mitochondrial dependent intrinsic cascade pathway. CgAgNPs could be possibly involved in the upregulation of *BAX* gene expression that leads to its activation and dimerization at the outer membrane of mitochondria causing permeabilization and ultimately leading to apoptosis. Bcl-2 act as an antagonist in the apoptotic machinery pathway whereas Bax promotes apoptosis acting as agonists by competing with Bcl-2.[91] Thus, in response to nuclear damage, the tumor suppressor protein p53 targets both Bcl-2 and Bax which triggers apoptosis and cell cycle inhibition.[92] Hence, CgAgNPs treated breast cancer cells may prove to be supporting evidence for inducing apoptotic cell death and provide an efficient way in combating progression of cancer. The p21, oncogenic cell cycle inhibitor protein mediates growth inhibition *via* p53 dependent apoptotic pathway. p21 inhibit CDKs (cyclin dependent kinases) which are essential for cell cycle growth.[93] Thus, its upregulation

promotes regression of breast cancer cells. Apoptosis or PCD is also regulated by Fas mediated signaling. The acquisition of FADD triggers Fas mediated apoptosis which recruits and activate caspase-8 to form homodimers and transmit death signal through caspase-3.[94] The cleavage of BH3-interacting domain death agonist (Bid) by caspase-8 causes porosity in mitochondrial membrane leading to cytosolic release of cytochrome c, thus ultimately leads to activation of downstream caspases on interaction with apoptotic protease activating factor (Apaf).[95] Thus, the present result demonstrates that the CgAgNPs treated breast cancer cells, MDA-MB-231 and MCF-7 cells triggers differential expression of proapoptotic genes (*BAX*, *P21* and *P53*), anti-apoptotic gene (*BCL-2*) and *FADD* gene responsible for intrinsic as well as extrinsic apoptotic pathway. Previous study has evidenced that the green mediated synthesis of AgNPs from *Gossypium hirsutum* induces apoptosis in A549 lung cancer cells through down regulation of *BCL-2* and enhanced expression of *BAX* genes.[88] The AgNPs mediated synthesis from aqueous extract of *Bergenia ligulata* in MCF-7 leads to cell cycle arrest due to upregulation of phosphorylated p53 and ROS generation that ultimately induces apoptosis.[96] Thus, the present study has been found in accordance with the previous researches and shows the potential chemotherapeutic action of CgAgNPs and role of apoptosis mediated biomarker genes on treated breast cancer cells.

4. Conclusion

Fungal endophyte mediated green silver nanoparticles have provided striking approach facilitating for biomedical and therapeutic interventions. The present study revealed the fungal endophyte *C. gloeosporioides* isolated from the *O. indicum* as a potential source for the fabrication of green silver nanoparticles exhibiting potential cytotoxic and anti-proliferative activities against human breast cancer cells. The preliminary

detection showed a visible colour change and UV-Visible spectral analysis showed characteristic peak in the wavelength range of 400–450 nm. The FT-IR spectroscopy analysis depicts the presence of functionalized fungal biomolecules carrying hydroxyl, carbonyl and free amino group that might be responsible for capping and stabilizing the silver nanoparticles. The crystallite size and purity were further confirmed by XRD analysis. The microscopic techniques such as AFM, FESEM and TEM depicts the agglomeration, size, surface topology as well as shape of the synthesized CgAgNPs. Further, CgAgNPs exhibited significant antiproliferative activity against human breast cancer cells, MDA-MB-231 and MCF-7 that was observed through reduction in cell viability in a dose-dependent manner. The cytotoxic activity of CgAgNPs against breast cancer cells was further validated through alteration in biochemical parameters. The reduced glucose uptake, reduced cell proliferation, and increased release of LDH in CgAgNPs treated breast cancer cells further confirms its cytotoxic and antiproliferative activity. The gene expression analysis revealed the upregulation of pro-apoptotic genes (*BAX* and *FADD*) cell cycle inhibitor gene (*P21*) and tumor suppressor gene (*P53*), while downregulation of anti-apoptotic gene (*BCL-2*). Collectively, this differential expression of genes provides the compelling evidence for the apoptosis inducing potential of the synthesized nanoparticle CgAgNPs. In summary, the synthesized CgAgNPs exhibit promising antiproliferative and cytotoxic effects against human breast cancer cells, highlighting their significant potential for translational studies in animal models and for the development of nano-based drugs.

Author contributions

Priyamvada Gupta: data curation; formal analysis; investigation; methodology; roles/writing-original draft; writing-review & editing; visualization. **Swati Singh:** data curation; formal analysis; investigation; methodology; roles/writing-original draft; writing review & editing; visualization. **Nilesh Rai:** data curation; formal analysis; investigation; writing review & editing. **Ashish Verma:** data curation; formal analysis; investigation; writing review & editing. **Harshita Tiwari:** data curation; formal analysis; investigation; writing review & editing. **Swapnil C. Kamble:** Formal analysis; Data curation. **Hemant Kumar Gautam:** formal analysis; writing review and editing. **Vibhav Gautam:** conceptualization; methodology; formal analysis; funding acquisition; investigation; project administration; resources; software; writing review and editing.

Conflicts of interest

The corresponding author on behalf of all the authors declares no potential conflict of interest.

Acknowledgements

References

1 S. Bayda, M. Adeel, T. Tuccinardi, M. Cordani and F. Rizzolio, *Molecules*, 2019, **25**, 112.

2 H. Barabadi, M. A. Mahjoub, B. Tajani, A. Ahmadi, Y. Junejo and M. Saravanan, *J. Cluster Sci.*, 2019, **30**, 259–279.

3 H. Tiwari, N. Rai, S. Singh, P. Gupta, A. Verma, A. K. Singh, Kajal, P. Salvi, S. K. Singh and V. Gautam, *Bioengineering*, 2023, **10**, 760.

4 S. Ahmadi, M. Fazilati, S. M. Mousavi and H. Nazem, *J. Exp. Nanosci.*, 2020, **15**, 363–380.

5 P. Gupta, N. Rai, A. Verma and V. Gautam, *Med. Res. Rev.*, 2023, **44**, 138–168.

6 A. Malhotra, K. Dolma, N. Kaur, Y. S. Rathore, Ashish, S. Mayilraj and A. R. Choudhury, *Bioresour. Technol.*, 2013, **142**, 727–731.

7 N. Rai, P. Kumari Keshri, A. Verma, S. C. Kamble, P. Mishra, S. Barik, S. Kumar Singh and V. Gautam, *Mycology*, 2021, **12**, 139–159.

8 J. Wen, S. K. Okyere, S. Wang, J. Wang, L. Xie, Y. Ran and Y. Hu, *J. Fungi*, 2022, **8**, 205.

9 P. K. Keshri, N. Rai, A. Verma, S. C. Kamble, S. Barik, P. Mishra, S. K. Singh, P. Salvi and V. Gautam, *Mycol. Prog.*, 2021, **20**, 577–594.

10 N. Atri, N. Rai, A. K. Singh, M. Verma, S. Barik, V. Gautam and S. K. Singh, *J. Sci. Res.*, 2020, **64**, 127–133.

11 A. Verma, N. Rai, S. C. Kamble, P. Mishra, S. Barik, R. Kumar, S. K. Singh, P. Salvi and V. Gautam, *Traditional Medicine for Neuronal Health*, 2023, 82–102.

12 R. Kousar, M. Naeem, M. I. Jamaludin, A. Arshad, A. N. Shamsuri, N. Ansari, S. Akhtar, A. Hazafa, J. Uddin, A. Khan and A. Al-Harrasi, *Am. J. Cancer Res.*, 2022, **12**, 2897–2919.

13 A. Verma, N. Rai, P. Gupta, S. Singh, H. Tiwari, S. B. Chauhan, V. Kailashiya and V. Gautam, *Environ. Toxicol.*, 2023, **38**, 2509–2523.

14 N. Rai, P. Gupta, P. K. Keshri, A. Verma, P. Mishra, D. Kumar, A. Kumar, S. K. Singh and V. Gautam, *Appl. Biochem. Biotechnol.*, 2022, **194**, 3296–3319.

15 A. Verma, P. Gupta, N. Rai, R. K. Tiwari, A. Kumar, P. Salvi, S. C. Kamble, S. K. Singh and V. Gautam, *J. Fungi*, 2022, **8**, 285.

16 P. Gupta, A. Verma, N. Rai, A. K. Singh, S. K. Singh, B. Kumar, R. Kumar and V. Gautam, *ACS Chem. Biol.*, 2021, **16**, 2068–2086.

17 S. Barik, N. Rai, P. Mishra, S. K. Singh and V. Gautam, *Curr. Sci.*, 2020, **118**, 698–699.

18 N. Rai, P. Gupta, A. Verma, S. Singh, H. Tiwari, R. Kumar, S. K. Singh and V. Gautam, in *Handbook of Oncobiology: From Basic to Clinical Sciences*, ed. R. C. Sobti, N. K. Ganguly and R. Kumar, Springer Nature Singapore, Singapore, 2023, pp. 1–24, DOI: 10.1007/978-981-99-2196-6_70-1.

19 L. Wang, C. Hu and L. Shao, *Int. J. Nanomed.*, 2017, **12**, 1227–1249.

20 A. Gade, P. Bonde, A. Ingle, P. Marcato, N. Duran and M. Rai, *J. Biobased Mater. Bioenergy*, 2008, **2**, 243–247.

21 V. Ahluwalia, J. Kumar, R. Sisodia, N. A. Shakil and S. Walia, *Ind. Crops Prod.*, 2014, **55**, 202–206.

22 T. Akther, V. Mathipi, N. S. Kumar, M. Davoodbasha and H. Srinivasan, *Environ. Sci. Pollut. Res.*, 2019, **26**, 13649–13657.

23 M. Govindappa, M. Lavanya, P. Aishwarya, K. Pai, P. Lunked, B. Hemashekhar, B. Arpitha, Y. Ramachandra and V. B. Raghavendra, *Bionanosci.*, 2020, **10**, 928–941.

24 U. Munawer, V. B. Raghavendra, S. Ningaraju, K. L. Krishna, A. R. Ghosh, G. Melappa and A. Pugazhendhi, *Int. J. Pharm.*, 2020, **588**, 119729.

25 N. A. Razak, N. Abu, W. Y. Ho, N. R. Zamberi, S. W. Tan, N. B. Alitheen, K. Long and S. K. Yeap, *Sci. Rep.*, 2019, **9**, 1514.

26 K. Nohara, F. Wang and S. Spiegel, *Breast Cancer Res. Treat.*, 1998, **48**, 149–157.

27 R. L. Siegel, K. D. Miller, H. E. Fuchs and A. Jemal, *CA Cancer J. Clin.*, 2022, **72**, 7–33.

28 R. L. Siegel, K. D. Miller, H. E. Fuchs and A. Jemal, *CA Cancer J. Clin.*, 2021, **71**, 7–33.

29 P. S. Ward and C. B. Thompson, *Cancer cell*, 2012, **21**, 297–308.

30 D. Hanahan and R. A. Weinberg, *Cell*, 2011, **144**, 646–674.

31 M. A. Khajah, S. Khushaish and Y. A. Luqmani, *PLoS One*, 2022, **17**, e0272449.

32 R. L. Aft, F. W. Zhang and D. Gius, *Br. J. Cancer*, 2002, **87**, 805–812.

33 Y. Feng, Y. Xiong, T. Qiao, X. Li, L. Jia and Y. Han, *Cancer Med.*, 2018, **7**, 6124–6136.

34 P. Miao, S. Sheng, X. Sun, J. Liu and G. Huang, *IUBMB life*, 2013, **65**, 904–910.

35 S. Kim, J. E. Choi, J. Choi, K.-H. Chung, K. Park, J. Yi and D.-Y. Ryu, *Toxicol. In Vitro*, 2009, **23**, 1076–1084.

36 Y. G. Yuan, S. Zhang, J. Y. Hwang and I. K. Kong, *Oxid. Med. Cell. Longevity*, 2018, **2018**, 6121328.

37 K. L. Thu, I. Soria-Bretones, T. W. Mak and D. W. Cescon, *Cell cycle (Georgetown, Tex.)*, 2018, **17**, 1871–1885.

38 D. Acharya, S. Satapathy, J. J. Thathapudi, P. Somu and G. Mishra, *Mater. Technol.*, 2022, **37**, 569–580.

39 S. Zhang, H. Jiang, B. Gao, W. Yang and G. Wang, *Front. Cell Dev. Biol.*, 2021, **9**, 811585.

40 S. Asad, S. Supriya, C. Gopal and A. Absar, *Spectrochim. Acta, Part A*, 2013, **114**, 144–147.

41 H. Bagur, R. S. Medidi, P. Somu, P. J. Choudhury, C. S. Karua, P. K. Guttula, G. Melappa and C. C. Poojari, *Mater. Technol.*, 2022, **37**, 167–178.

42 R. S. Yehia and H. Al-Sheikh, *World J. Microbiol. Biotechnol.*, 2014, **30**, 2797–2803.

43 N. Rai, P. K. Keshri, P. Gupta, A. Verma, S. C. Kamble, S. K. Singh and V. Gautam, *PLoS One*, 2022, **17**, e0264673.

44 T. Mosmann, *J. Immunol. Methods*, 1983, **65**, 55–63.

45 D. P. Bonfim, C. V. Nakamura, J. X. de Araújo Júnior, G. L. Pessini, P. E. C. Leite, J. A. Morgado-Díaz and F. J. P. R. Leve, *Phytother. Res.*, 2021, **35**, 3769–3780.

46 V. Gautam, A. Singh, S. Yadav, S. Singh, P. Kumar, S. Sarkar Das and A. K. J. D. Sarkar, *Development*, 2021, **148**, dev190033.

47 S. A. Bustin, V. Benes, J. A. Garson, J. Hellemans, J. Huggett, M. Kubista, R. Mueller, T. Nolan, M. W. Pfaffl, G. L. Shipley, J. Vandesompele and C. T. Wittwer, *Clin. Chem.*, 2009, **55**, 611–622.

48 P. Mulvaney, *Langmuir*, 1996, **12**, 788–800.

49 C. Krishnaraj, E. G. Jagan, S. Rajasekar, P. Selvakumar, P. T. Kalaichelvan and N. Mohan, *Colloids Surf., B*, 2010, **76**, 50–56.

50 N. Rai, P. Gupta, A. Verma, S. K. Singh and V. Gautam, *BioFactors*, 2023, **49**, 663–683.

51 N. Rai, P. Gupta, A. Verma, R. K. Tiwari, P. Madhukar, S. C. Kamble, A. Kumar, R. Kumar, S. K. Singh and V. Gautam, *ACS omega*, 2023, **8**, 3768–3784.

52 S. Anil Kumar, M. K. Abyaneh, S. W. Gosavi, S. K. Kulkarni, R. Pasricha, A. Ahmad and M. I. Khan, *Biotechnol. Lett.*, 2007, **29**, 439–445.

53 H. Korbekandi, Z. Ashari, S. Iravani and S. Abbasi, *Iran. J. Pharm. Res.*, 2013, **12**, 289–298.

54 A. Ingle, A. Gade, S. Pierrat, C. Sonnichsen and M. Rai, *Curr. Nanosci.*, 2008, **4**, 141–144.

55 N. Vigneshwaran, N. M. Ashtaputre, P. V. Varadarajan, R. P. Nachane, K. M. Paralikar and R. H. Balasubramanya, *Mater. Lett.*, 2007, **61**, 1413–1418.

56 K. Anandalakshmi, J. Venugobal and V. Ramasamy, *Appl. Nanosci.*, 2016, **6**, 399–408.

57 R. Anith Jose, D. Devina Merin, T. S. Arulananth and N. Shaik, *J. Nanomater.*, 2022, **2022**, 4056551.

58 P. Khandel and S. K. Shahi, *J. Nanostruct. Chem.*, 2018, **8**, 369–391.

59 P. Azmath, S. Baker, D. Rakshith and S. Satish, *Saudi Pharm. J.*, 2016, **24**, 140–146.

60 K. Prabakaran, C. Ragavendran and D. Natarajan, *RSC Adv.*, 2016, **6**, 44972–44986.

61 K. I. Alsamhary, *Saudi J. Biol. Sci.*, 2020, **27**, 2185–2191.

62 A. Mahajan, A. Arya and T. S. Chundawat, *Synth. Commun.*, 2019, **49**, 1926–1937.

63 D. Arumai Selvan, D. Mahendiran, R. Senthil Kumar and A. Kalilur Rahiman, *J. Photochem. Photobiol., B*, 2018, **180**, 243–252.

64 J. Coates, *Encyclopedia of Analytical Chemistry*, 2000, 10815–10837.

65 D. Singh, V. Rathod, S. Ninganagouda, J. Hiremath, A. K. Singh and J. Mathew, *Bioinorg. Chem. Appl.*, 2014, **2014**, 408021.

66 A. Gole, C. Dash, V. Ramakrishnan, S. Sainkar, A. Mandale, M. Rao and M. Sastry, *Langmuir*, 2001, **17**, 1674–1679.

67 D. Wang, B. Xue, L. Wang, Y. Zhang, L. Liu and Y. Zhou, *Sci. Rep.*, 2021, **11**, 10356.

68 M. A. Yassin, A. M. Elgorban, A. E.-R. M. A. El-Samawaty and B. M. A. Almunqedhi, *Saudi J. Biol. Sci.*, 2021, **28**, 2123–2127.

69 V. S. Kotakadi, S. A. Gaddam, S. K. Venkata, P. V. G. K. Sarma and D. V. R. Sai Gopal, *3 Biotech*, 2016, **6**, 216.

70 T. Singh, K. Jyoti, A. Patnaik, A. Singh, R. Chauhan and S. S. Chandel, *J. Genet. Eng. Biotechnol.*, 2017, **15**, 31–39.

71 G. Li, D. He, Y. Qian, B. Guan, S. Gao, Y. Cui, K. Yokoyama and L. Wang, *Int. J. Mol. Sci.*, 2012, **13**, 466–476.

72 P. Gupta, N. Rai, A. Verma, D. Saikia, S. P. Singh, R. Kumar, S. K. Singh, D. Kumar and V. Gautam, *ACS omega*, 2022, **7**, 46653–46673.

73 N. Ahmad, S. Sharma, M. K. Alam, V. N. Singh, S. F. Shamsi, B. R. Mehta and A. Fatma, *Colloids Surf., B*, 2010, **81**, 81–86.

74 M. Manjunath Hulikere and C. G. Joshi, *Process Biochem.*, 2019, **82**, 199–204.

75 P. Salvi, H. Mahawar, R. Agarrwal, V. Gautam and R. Deshmukh, *Front. Microbiol.*, 2022, **13**, 3407.

76 H. Du, T. M. Lo, J. Sitompul and M. W. Chang, *Biochem. Biophys. Res. Commun.*, 2012, **424**, 657–662.

77 S. Gurunathan, J. W. Han, V. Eppakayala, M. Jeyaraj and J.-H. J. B. R. I. Kim, *BioMed Res. Int.*, 2013, **2013**, 1–10.

78 S. V. Otari, S. H. Pawar, K. S. P. Sanjay, K. S. Raushan, K. Sang-Yong, L. Jai Hyo and Z. Liaoyuan, *J. Microbiol. Biotechnol.*, 2017, **27**, 731–738.

79 M. J. Lee, S. J. Lee, S. J. Yun, J.-Y. Jang, H. Kang, K. Kim, I.-H. Choi and S. Park, *Int. J. Nanomed.*, 2016, 55–68.

80 M. Zuberek, D. Wojciechowska, D. Krzyzanowski, S. Meczynska-Wielgosz, M. Kruszewski and A. Grzelak, *J. Nanobiotechnol.*, 2015, **13**, 72.

81 M. Feoktistova, P. Geserick and M. Leverkus, *Cold Spring Harb. Protoc.*, 2016, **2016**, 343–346.

82 M. A. Feitelson, A. Arzumanyan, R. J. Kulathinal, S. W. Blain, R. F. Holcombe, J. Mahajna, M. Marino, M. L. Martinez-Chantar, R. Nawroth, I. Sanchez-Garcia, D. Sharma, N. K. Saxena, N. Singh, P. J. Vlachostergios, S. Guo, K. Honoki, H. Fujii, A. G. Georgakilas, A. Bilsland, A. Amedei, E. Niccolai, A. Amin, S. S. Ashraf, C. S. Boosani, G. Guha, M. R. Ciriolo, K. Aquilano, S. Chen, S. I. Mohammed, A. S. Azmi, D. Bhakta, D. Halicka, W. N. Keith and S. Nowsheen, *Semin. Cancer Biol.*, 2015, **35**(Suppl), S25–s54.

83 S. Gurunathan, M. Qasim, C. Park, H. Yoo, J.-H. Kim and K. Hong, *BioMed Res. Int.*, 2018, **19**, 2269.

84 R. Mata, J. R. Nakkala and S. R. Sadras, *Colloids Surf., B*, 2015, **128**, 276–286.

85 Y. S. Lee, D. W. Kim, Y. H. Lee, J. H. Oh, S. Yoon, M. S. Choi, S. K. Lee, J. W. Kim, K. Lee and C.-W. Song, *Arch. Toxicol.*, 2011, **85**, 1529–1540.

86 D. Bhatia, A. Mittal and D. K. Malik, *Indian J. Exp. Biol.*, 2021, **15**, 427–440.

87 J. Tower, *Ageing Res. Rev.*, 2015, **23**, 90–100.

88 N. Kanipandian, D. Li and S. Kannan, *Biotechnol. Rep.*, 2019, **23**, e00339.

89 M. A. Anderson, J. Deng, J. F. Seymour, C. Tam, S. Y. Kim, J. Fein, L. Yu, J. R. Brown, D. Westerman and E. G. Si, *Blood, The Journal of the American Society of Hematology*, 2016, **127**, 3215–3224.

90 F. Bray, J. S. Ren, E. Masuyer and J. Ferlay, *Int. J. Cancer*, 2013, **132**, 1133–1145.

91 J. M. Hardwick and L. Soane, *Cold Spring Harbor Perspect. Biol.*, 2013, **5**, a008722.

92 A. Basu and S. Haldar, *Mol. Hum. Reprod.*, 1998, **4**, 1099–1109.

93 J. W. Harper, G. R. Adami, N. Wei, K. Keyomarsi and S. Elledge, *Cell*, 1993, **75**, 805–816.

94 A. M. Chinnaiyan, K. O'Rourke, M. Tewari and V. M. Dixit, *Cell*, 1995, **81**, 505–512.

95 K. Huang, J. Zhang, K. L. O'Neill, C. B. Gurumurthy, R. M. Quadros, Y. Tu and X. Luo, *J. Biol. Chem.*, 2016, **291**, 11843–11851.

96 P. Takáč, R. Michalková, M. Čižmáriková, Z. Bedlovičová, Ľ. Balážová and G. Takáčová, *Life*, 2023, **13**.